Available online at www.sciencedirect.com
ScienceDirect
Scripta Materialia 64 (2011) 1031–1034
Scripta MATERIALIA
www.elsevier.com/locate/scriptamat

Effect of crystalline metallic particles on the compressive behavior of a cellular amorphous metal

Alan H. Brothers,[a] Benjamin Mangrich,[b] Marie Cox[b,*] and David C. Dunand[b]

[a] *Western Digital Co. Ltd., Klongjig, BangPa-In, Ayuthaya 13160, Thailand*
[b] *Department of Materials Science and Engineering, Northwestern University, Evanston, IL 60208, USA*

Received 14 January 2011; accepted 12 February 2011
Available online 18 February 2011

Molten Vit106 ($Zr_{57}Nb_5Cu_{15.4}Ni_{12.6}Al_{10}$) was infiltrated into a BaF_2 preform containing W particles, and quenched. Salt dissolution resulted in an open-porosity foam with struts consisting of amorphous Vit106 containing crystalline W particles. This composite foam exhibits high compressive strains (~75%), a low plateau stress (~30 MPa) and higher damage accumulation than prior single-phase Vit106 foams. Likely explanations are the lower porosity in the composite foam (43% vs. 76%), damage from galvanic corrosion during salt removal, and tungsten embrittlement during processing.

Keywords: Bulk metallic glass; Porous material; Foams; Composites; Acoustic methods

For many years, the only method known to ductilize brittle bulk metallic glasses (BMG) was to inhibit shear band motion by dispersing a reinforcement phase in the glass, i.e. by fabricating a metallic-glass-matrix composite (MGMC) [1–3]. More recently, several groups have demonstrated that pores are also effective at ductilizing BMG [4–7] (i) by creation of stable shear bands during bending of long, slender struts in high-porosity BMG foams [8] and (ii) by formation of a complex multiaxial stress state between neighboring pores of lower porosity foams [9,10]. Porous and foamed BMG have lower stiffness and strength compared to fully dense MGMC, but also offer fewer obstacles to deformation and therefore achieve unmatched compressive strains of up to 80% [4]. These two different approaches towards ductilizing BMG (i.e. ductile second phases and pores) are independent, so it is interesting to use them simultaneously by creating a porous MGMC. This approach has been demonstrated in a syntactic foam (consisting of hollow crystalline steel spheres within an amorphous Mg-based BMG) exhibiting macroscopic plasticity due to the ductile steel shells despite significant small-scale fracture within the brittle BMG phase [11]. The BMG matrix was present in large, low-aspect ratio features that were well separated from any ductile steel; since ductility is promoted by high local aspect ratios and ductile reinforcements, it seemed likely that the extensive small-scale fracture in this foam could be mitigated by ensuring longer, more slender BMG features and more intimate dispersion of the crystalline second phase. The present work pursues this concept by creating and studying a composite BMG foam (i.e. a MGMC foam), which better meets these requirements by reducing pore and feature size and by more intimately mixing the phases. More specifically, a salt-replicated BMG foam structure (known to promote significant plasticity in single-phase BMG [12]) is created that incorporates a ductile crystalline tungsten powder within the BMG (also known from earlier work reviewed above to promote plasticity [1–3]).

The composite foam was produced from three components: an amorphous $Zr_{57}Nb_5Cu_{15.4}Ni_{12.6}Al_{10}$ (Vit106) ingot, 99.95% crystalline W powder with 45–150 μm size, and 99.999% BaF_2 powder with 212–250 μm size. The BaF_2 and W powders were mixed in a 70:30 volume ratio and the blend was poured into a stainless steel crucible of 6.5 mm inner diameter. The powder blend was lightly tapped to promote settling without inducing density- or size-based separation of the W and BaF_2. A charge of Vit106 was suspended above the powder bed in a W wire basket.

The bottom of the crucible (which was evacuated to a 4 mPa residual pressure) was placed in a furnace to eliminate volatiles from the powder preform and to preheat it to the infiltration temperature of 1000 °C. After

* Corresponding author. E-mail: mcox@u.northwestern.edu

1359-6462/$ - see front matter © 2011 Acta Materialia Inc. Published by Elsevier Ltd. All rights reserved.
doi:10.1016/j.scriptamat.2011.02.014

15 min, the Vit106 charge was lowered onto the preheated preform and allowed to melt under vacuum. After 5 min, high-purity argon with 100 kPa positive pressure was admitted to the crucible, providing a net 200 kPa pressure gradient to drive infiltration of the molten Vit106 into the BaF_2/W powder preform. After 1 min, the crucible was plunged into a chilled brine solution to vitrify the Vit106. The infiltrated specimen was machined into a cylindrical compressive sample (3.0 mm diameter, 4.9 mm height) using a diamond wheel and diamond wafering saw. The BaF_2 was then removed in ultrasonically agitated 2 M HNO_3 containing 70 g L^{-1} of 22 ± 5 μm alumina powder as a corrosion inhibitor and held at 50–55 °C, as described elsewhere [13]. Full removal of the salt, as indicated by a stable density measured using He pycnometry, took just over 80 h.

Compressive mechanical properties of the sample were measured using an MTS servohydraulic universal testing system at a constant nominal strain rate of 10^{-4} s^{-1}. Compression was applied using hardened tool steel pistons with a lubricated steel sleeve to ensure parallelism, and the strain was calculated from the crosshead displacement after correction for load train compliance using calibration data taken before and after testing.

Acoustic emissions (AEs) were measured during the compression test by three broadband piezoelectric transducers (Deci Model SE9125-M) coupled with silicone grease, one on each platen and the third fixed to the upper piston. AE events were recorded after preamplification (34 dB) using a Vallen AMS5 acoustic emissions test system. The measurement time resolution was 0.1 μs, the rearm time was 3.2 ms and the triggering threshold was 30.3 dB relative to a 1 μV transducer output before preamplification. To minimize attenuation, silicone grease was also applied to both specimen/piston interfaces. Events were filtered using a 2 ms discrimination time to eliminate events detected first at either of the guard-transducers located on the platens, i.e. to eliminate events originating from outside the gauge region. The measurement method was the same described in previous work [13], except that a newer (AMS5 vs. AMS3) test system was used and events with amplitude <33.7 dB (rather than 30.7 dB) were removed.

Though the present Vit106/W composite foam was processed under very similar conditions to earlier Vit106 foams [13], addition of W powders into the preforms required some changes in processing. Most importantly, it forbade the usual powder preform sintering step because the vapor-dominated BaF_2 sintering mechanism posed a risk of coating W surfaces with BaF_2 and thereby undermining the eventual Vit106/W interface strength. Attempts to circumvent the problem by cold-pressing led to tightly packed preforms prone to incomplete infiltration, so loose preforms were necessary.

Because the sintered necks that normally assured percolation of the BaF_2 were absent, it was necessary to choose W/BaF_2 particle size and volume ratios carefully to allow complete salt removal after infiltration while promoting W engulfment by the melt. Fine W powders and low W fractions failed to produce uniform W/BaF_2 mixtures, and resulted in undesirable redistribution of the W powders during infiltration. Coarse W powders and high W fractions disrupted salt packing and therefore salt removal. The particle sizes and fractions used here reflect a compromise between these effects, but the absence of sintering and the interference of the W combined to produce higher relative density in the foam. The bulk density of the foam discussed below was measured by Archimedes' method to be 5.5 ± 0.1 g cm^{-3}, while the density of the solid composite phase in the foam was measured by He pycnometry to be 9.7 ± 0.4 g cm^{-3}. The corresponding foam relative density and porosity are estimated at $57 \pm 3\%$ and $43 \pm 3\%$, respectively. Since only the BaF_2 powders contribute to foam porosity, this implies a lower BaF_2 packing density of $43 \pm 3\%$, compared to $50 \pm 2\%$ in earlier W-free sintered BaF_2 patterns [13]. The densities reveal a W content of 23 vol.% within the Vit106 and a porosity-to-W volume ratio of 77:23. The increase in porosity-to-W ratio over the original BaF_2-to-W ratio (70:30) indicates that some solid mass (Vit106 and/or W) was lost during processing.

Fig. 1a shows a scanning electron microscope (SEM) image of the composite foam surface prior to deformation. The foam has visibly higher relative density and blockier (lower aspect ratio) solid features than prior W-free Vit106 foams [13], a result of the disruption in salt packing described above. The inset in Fig. 1a shows an individual strut within the foam, with the Vit106 ma-

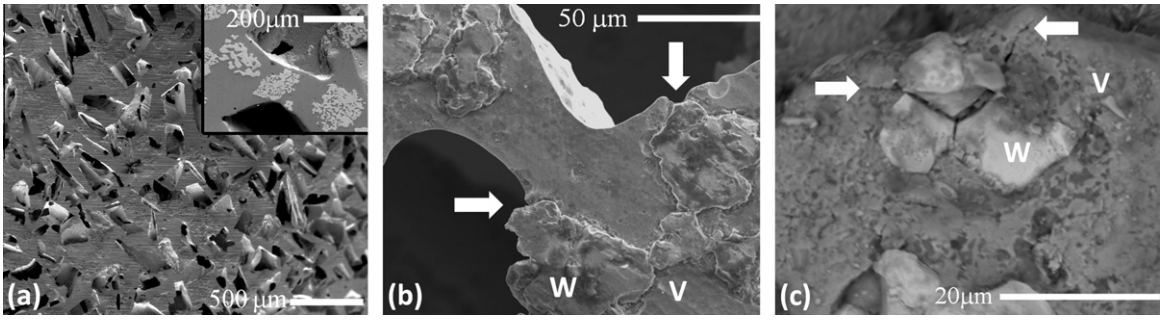

Figure 1. SEM images. (a) The Vit106/W composite foam surface. The inset shows a magnified strut consisting of W particles clusters constituting individual powders (light gray contrast) in a Vit106 matrix (dark gray contrast). (b) A strut within the composite foam, after salt removal and before deformation. Arrows indicate regions where the interface between Vit106 (V) and tungsten (W) has been corrosively attacked. (c) A fracture surface within the composite foam after deformation. Arrows indicate cracks that appear to originate from the tungsten (W) particles and propagate into, and stop within, the Vit106 (V) matrix.

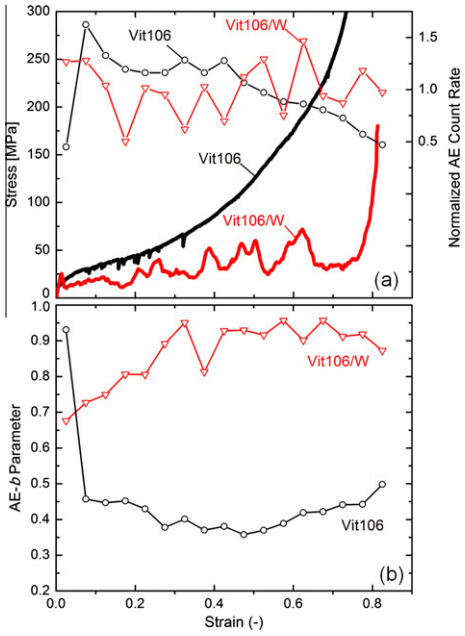

Figure 2. (a) Compressive stress–strain curves and strain dependence of normalized AE count rates for Vit106 foam [13] and Vit106/W composite foam with relative densities of 24% and 57%, respectively. (b) Comparison of AE-*b* values between the Vit106/W composite foam and the Vit106 foam [13], as functions of strain. To ensure the most direct comparison, the Vit106 foam data [13] were reanalyzed using the same analysis methods used with the present data for the Vit106/W composite foam.

trix and embedded W particles clearly visible. The latter are quite porous, having been synthesized by sintering of smaller powders. Based on the analysis of several such images, 20% of W particles were dense, while the remainder had 31 ± 5% porosity. As shown in Fig. 1a, Vit106 infiltrated this porosity thoroughly, indicative of good wetting.

Compressive stress–strain curves for the prior Vit106 foam (3.55 mm diameter, 7.6 mm height [13]) and the present Vit106/W composite foam are shown in Fig. 2a. The Vit106 foam shows behavior reminiscent of a ductile foam, with a yield stress of 27 MPa and a smoothly rising plateau region leading into densification at high strain, though several sharp serrations occur early in the plateau. The Vit106/W composite foam shows near-linear loading to 25 MPa, followed by a stress drop. Thereafter, the curve rises and falls around an average stress near 32 MPa until about 75% strain, at which point densification begins. Its behavior is reminiscent of a semi-brittle foam, and large fragments broke off occasionally during the test, the first of which was visible at ~15% strain.

The normalized acoustic emission count rates for both foams are shown in Fig. 2a, where the AE data were separated into populations of 5% intervals of applied strain and normalized by the average count rate (7117 for Vit106/W, 1065 for Vit106). The average count rate for the Vit106 foam was fairly low at 1065 and diminished with increasing strain, while rates in the composite foam were much higher and more erratic. Overlaying the composite foam stress and count rate data shows a strong correlation between flow stress

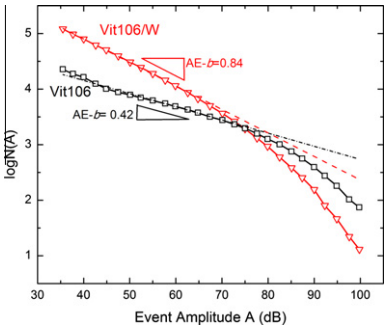

Figure 3. Cumulative event amplitude distributions for the Vit106 foam [13] and Vit106/W composite foam, including events taken at all values of strain. Slopes are the AE-*b* parameters.

and AE activity. Wherever the foam gains/loses stress, AE activity increases/decreases.

To better elucidate the underlying causes of the AE activity shown in Fig. 2, the data were analyzed using the Gutenberg–Richter (GR) method [14]. A detailed description of this method is provided in an earlier publication [13]; in short, the GR method fits AE data, plotted as cumulative AE counts (for the whole compressive test) vs. AE amplitude (Fig. 3), to a power-law described by two parameters, *a* and *b*, where the parameters are fitted using data of amplitude <65 dB to avoid sample size affects. The AE-*a* parameter is the intercept of the distribution and is therefore quite sensitive to experimental variables such as acoustic attenuation and detector sensitivity. The AE-*b* parameter is derived from the negative of the slope of the distribution, i.e. the power law exponent by which AE activity decays with increasing amplitude, and is more characteristic of the material being tested. Larger values of AE-*b* reflect AE activity with fewer high-amplitude fractures (a distribution that decays quickly with increasing amplitude), while smaller values of AE-*b* reflect activity with comparatively more highly energetic fractures (an amplitude distribution that stays flatter) [15].

The evolution of AE-*b* with strain for the Vit106 and Vit106/W composite foams is shown in Fig. 2b. As might be expected based on the AE-*b* values for the overall distributions in Fig. 3 (0.42 and 0.84), AE-*b* values are consistently much lower in the Vit106 foam than in the composite foam, suggesting that proportionally fewer high-energy strut fractures occurred in the composite. The most straightforward explanation for this effect is that the W particles acted as stress concentrators, weakening and embrittling the struts in the composite foam and thus producing an abundance of low-energy fractures at the expense of high-energy fractures.

Scanning electron micrographs of the foam before and after compression support this explanation. Prior to compression (Fig. 1b), corrosion pits are present near the Vit106/W interfaces, most probably due to galvanic attack of Vit106 during salt removal. Following compression (Fig. 1c), cracks are visible at the boundaries between the small W particle clusters constituting individual powders (Fig. 1a). The fact that some of these cracks correspond to short, arrested cracks in the surrounding Vit106 suggests that they nucleated in the W

and then spread into the Vit106, but in situ observation is needed to confirm this hypothesis.

In addition to the differing magnitudes of AE-*b* between the foams, the trends are opposing: AE-*b* for the Vit106 foam decreases throughout the early plateau region, while AE-*b* for the composite foam increases over the same interval. In the Vit106 foam, strength and ductility are negatively correlated, with the thinner, longer struts being both weaker and more ductile, and the thicker, shorter struts being stronger but more brittle. Conversely, in the composite foam, strength and ductility are probably positively correlated, because struts containing W are both weakened and embrittled by the associated flaws (Fig. 1b), while struts lacking W remain both maximally strong and ductile.

The different trends in AE-*b* values in Fig. 2b may thus be rationalized as follows: the Vit106 foam consisted of a large number of weak, ductile (slender) struts in parallel with a few strong, brittle (squat) struts. During compression, the high volume fraction of slender struts allowed them to carry high total loads despite their individual weakness. Failure in any such strut only marginally increased the load on its neighbors, so the ductile struts continued deforming and fracturing gradually until enough had shed their loads onto the stronger, brittle struts to make them fail. In this way, the more numerous, ductile struts, despite their lower strength, "protected" the minority of stronger, brittle struts. The AE-*b* value decreased with strain, as the protection of the ductile struts wore out and more of the strong, brittle struts were loaded to failure.

By contrast, the composite foam consisted of a large number of weaker, more brittle (W-bearing) struts, in parallel with a few stronger, more ductile (W-free) struts. As before, the weaker struts dominated at low strains due to their larger volume fraction but, because these weaker struts were also more brittle, they shed their load more rapidly onto the smaller population of strong struts. The higher strength and ductility of these stronger struts allowed them to "protect" the majority for a time, resulting in some increase in load-bearing capacity. However, their low numbers still limited the foam to comparatively low loads, and their eventual failure initiated unstable collapse by redistributing the loads back onto the surrounding weak, brittle majority. With their "protection" exhausted, those brittle struts rapidly fractured, leading to a drop in flow stress that was not recovered until stress had built up in another region of the foam. In this way, the strongest struts were loaded earlier in the deformation and exhausted more quickly, leading to an increase in AE-*b*.

While the embrittling effects of W addition were unexpected, understanding of the mechanisms at play suggests several steps to improve this situation in future work. First, foam relative density should be decreased. Previous results from W-free Vit106 foams show that low relative density correlates to lower microfracture activity, due to thinner, more ductile struts [8]. Second, the reinforcement should be chosen to minimize galvanic attack at the interface, or measures like corrosion inhibitors or galvanic protection used to eliminate it altogether. Third, dense reinforcement particles, rather than porous sintered particles like those used here, should be used to eliminate crack nucleation from within the reinforcement. Devising a means of keeping reinforcement particles thoroughly embedded within the struts would serve the dual purpose of suppressing galvanic interactions and mitigating the effects of cracking in the reinforcement. Finally, a reinforcement with less propensity for recrystallization can be chosen [16] (W wire baskets used in processing the foams were found to be much less ductile than unused baskets). With these simple changes, it should be possible to restore the intended ductilizing function of the crystalline reinforcement and achieve BMG foams with two independent types of ductilizing mechanisms at play simultaneously: porosity and ductile second phases.

The authors thank the Infrastructure Technology Institute (ITI) at Northwestern University for use of their acoustic equipment and David Prine (ITI) for his invaluable help with the AE measurements.

[1] D.C. Hofmann, J. Suh, A. Wiest, G. Duan, M. Lind, M.D. Demetriou, W.L. Johnson, Nature 451 (2008) 1085–1089.
[2] E.S. Park, D.H. Kim, Met. Mat. Int. 11 (2005) 19–28.
[3] J. Lewandowski, M. Shazly, A. Shamimi Nouri, Scripta Mater. 54 (2006) 337–341.
[4] A. Brothers, D. Dunand, MRS Bull. 32 (2007) 639–643.
[5] A.H. Brothers, D.C. Dunand, Adv. Mater. 17 (2005) 484–486.
[6] T. Wada, A. Inoue, Mater. Trans. 44 (2003) 2228–2231.
[7] M.D. Demetriou, C. Veazey, J.S. Harmon, J.P. Schramm, W.L. Johnson, Phys. Rev. Lett. 101 (2008) 145702.
[8] A. Brothers, D. Dunand, Acta Mater. 53 (2005) 4427–4440.
[9] T. Wada, M. Kinaka, A. Inoue, J. Mater. Res. 21 (2006) 1041–1047.
[10] A. Inoue, T. Wada, D.V. Louzguine-Luzgin, Mat. Sci. Eng. A 471 (2007) 144–150.
[11] A.H. Brothers, D.C. Dunand, Q. Zheng, J. Xu, J. Appl. Phys. 102 (2007) 23508.
[12] A. Brothers, D. Dunand, Scripta Mater. 54 (2006) 513–520.
[13] A. Brothers, D. Prine, D. Dunand, Intermetallics 14 (2006) 857–865.
[14] B. Gutenberg, C.F. Richter, B. Seismol, Soc. Am. 32 (1942) 163.
[15] J. Aue, J.T.M. De Hosson, J. Mater. Sci. 33 (1998) 5455–5462.
[16] E. Lassner, W. Schubert, Tungsten, Plenum Press, New York, 1999.